

NUMERICAL SIMULATIONS OF FLOOD PROPAGATION IN A FLOODPLAIN WITH STRUCTURES

By

Mirei SHIGEDA, Juichiro AKIYAMA, Masaru URA

Department of Civil Engineering, Kyushu Institute of Technology
Sensuicho 1-1, Tobata, Kitakyushu 804-8550, JAPAN

Akhilesh Kumar JHA

Former Department of Civil Engineering, Kyushu Institute of Technology
Sensuicho 1-1, Tobata, Kitakyushu 804-8550, JAPAN

and

Yoshitaka ARITA

Ministry of Land, Infrastructure and Transport,
Shikoku Regional Development Bureau, Nakamura 210, Osu 795-8512, JAPAN

SYNOPSIS

A first-order accurate Finite-Volume Method(FVM) numerical model for 2D flood flows is presented. The model uses an unstructured triangular grid system and incorporates conservative properties as well as a signal propagation through the Flux-Difference Splitting(FDS) technique. To test the reliability of the model, experiments on dam-break flood waves propagating in a channel as well as a floodplain with structures were conducted. The depths and the surface velocities of flood flows were measured by means of image analysis and Particle Tracking Velocimetry(PTV), respectively. The model verifications against these experimental data show that the proposed model can reproduce flood flows with structures with reasonable accuracy.

INTRODUCTION

The frequency of the occurrence of high intensity rainfall and subsequent flash floods has been increasing in many parts of the world. As a result, even densely populated and well-developed areas suffer from serious flooding. To mitigate flood damage, countermeasures need to be improved against flooding, such as more reliable hazard maps and more effective systems of emergency evacuation, in addition to better flood control facilities such as diversion channels and flood retarding basins. These countermeasures are commonly constructed according to prediction results of flood-flow behavior based on numerical simulations of flood propagation.

A numerical model for simulating flood flows, which is usually influenced by complicated floodplain geometries with structures, road networks and buildings, is required. Such effects are commonly incorporated into a model through a grid arrangement, which conforms to the boundaries in the interior and around the computational domain, together with suitable conditions describing the type of the boundary. Therefore, two factors in constructing an accurate numerical model for

flood flows become important: First a numerical technique for integration of governing equations, and second a suitable grid system to implement that numerical technique on.

Numerical techniques using Finite-Volume Method(FVM) based on Flux-Difference Splitting(FDS) have been found to provide accurate results in cases of the 2D shallow water equations for modeling flood flows (e.g. (2), (6), (9), (11)). The FVM is based on the integral form of the governing equations. This method uses the total normal flux through the control-volume boundaries for marching in time. The FDS is one of the most reliable and accurate techniques used to estimate numerical flux. This technique essentially applies the upwind difference method to the linearized Riemann problem (10). While this technique can determine the directionality of signal propagation, the approximate Jacobian developed by Roe (10) enables conservative splitting of flux-differences. Although the rigorous theoretical development for FDS has been confined to 1D flows, its logical extension for solving 2D problems reported in the above literature show significant advantages.

Most of the existing models have used a structured grid system ((2), (6),(9)), while a few models have used an unstructured grid system((7),(8),(11)). In an unstructured grid system, the grid size may vary in the computational domain depending on the local geometry. This makes the work of laying out of grids around a complicated geometry easier than a structured grid system. An unstructured grid system is also advantageous in that it reduces computation time for comparable accuracy. However, data on the actual accuracy and applicability of the numerical models based on an unstructured grid system for 2D flood flows is rather inadequate. To make a complete and quantitative verification of the models, reliable experimental data of flood flows should be obtained.

Experiments on flood flows have been conducted (e.g. (3), (4), (5),(12)). Among these studies, Bellos et al. (4) and Fraccarollo and Toro (5) specified the inflow condition, and these experimental data appear to be reliable. Bellos et al. (4) have provided experimental data on the flow depths of 2D dam-break flows in a converging-diverging channel, which separated the reservoir section from the floodplain section. The finite depth in the reservoir section and dry- or wet-bed condition in the floodplain section were given as the initial inflow condition. Fraccarollo and Toro (5) provided experimental data for flow depth and velocity for propagation of 2D dam-break flood wave in a floodplain due to opening a gate, which separate the reservoir section from the floodplain section. The finite depth in the reservoir section and dry-bed condition in the floodplain section were given as the initial inflow conditions. In these experiments, the slope of the channel or the floodplain were changed but remained featureless. According to our findings, experimental data on the flow depths and velocities of flood propagating in a floodplain with structures or with complicated floodplain geometry as well as reliable inflow conditions have not been reported.

In this paper, a high-accuracy numerical model for 2D flood flows with capability to handle a complicated floodplain geometry is presented. This model is based on FVM and FDS techniques (10), satisfying conservative property while incorporating signal propagation. An unstructured triangular grid system is employed for enhancing practical applicability. To test the reliability of this model, experiments on flood propagation in a channel and a floodplain with structures were conducted. The quantitative accuracy and applicability of the model are verified against these experimental data. Findings shows that the proposed model can reproduce the observed depth and velocities of the flood propagation with reasonable accuracy.

GOVERNING EQUATIONS

The governing equations for 2D flood flows can be expressed as

$$\frac{\partial \mathbf{U}}{\partial t} + \frac{\partial \mathbf{E}}{\partial x} + \frac{\partial \mathbf{F}}{\partial y} + \mathbf{S} = \mathbf{0} \quad (1)$$

where \mathbf{U} = flow vector; \mathbf{E} and \mathbf{F} = flux vectors; \mathbf{S} = vector containing source and sink terms. These vectors are given by

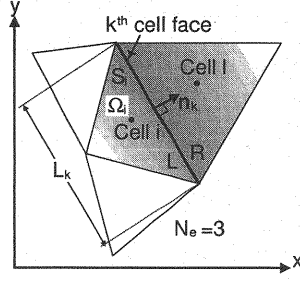


Fig.1 Control Volume

$$\begin{aligned}
 \mathbf{U} &= \begin{pmatrix} h \\ uh \\ vh \end{pmatrix}; \mathbf{E} = \begin{pmatrix} uh \\ u^2h + \frac{1}{2}gh^2 \\ uvh \end{pmatrix}; \\
 \mathbf{F} &= \begin{pmatrix} vh \\ uvh \\ v^2h + \frac{1}{2}gh^2 \end{pmatrix}; \mathbf{S} = \begin{pmatrix} 0 \\ -gh(S_{ox} - S_{fx}) \\ -gh(S_{oy} - S_{fy}) \end{pmatrix}
 \end{aligned} \quad (2)$$

where h = flow depth; u, v = flow velocities along x - and y -direction, respectively; g = acceleration due to gravity; S_{ox} and S_{oy} = bed slopes along x - and y -direction, respectively; S_{fx} and S_{fy} = friction slopes along x - and y -direction, respectively. The friction slopes are estimated as

$$S_{fx} = \frac{n^2 u \sqrt{u^2 + v^2}}{h^{4/3}}; \quad S_{fy} = \frac{n^2 v \sqrt{u^2 + v^2}}{h^{4/3}} \quad (3)$$

where n = Manning's roughness coefficient.

The flux vectors \mathbf{E} and \mathbf{F} are related to \mathbf{U} through their Jacobian matrices \mathbf{A} and \mathbf{B} as

$$\mathbf{A} = \frac{\partial \mathbf{E}}{\partial \mathbf{U}} = \begin{pmatrix} 0 & 1 & 0 \\ -u^2 + c^2 & 2u & 0 \\ -uv & v & u \end{pmatrix}; \quad \mathbf{B} = \frac{\partial \mathbf{F}}{\partial \mathbf{U}} = \begin{pmatrix} 0 & 0 & 1 \\ -uv & v & u \\ -v^2 + c^2 & 0 & 2v \end{pmatrix} \quad (4)$$

where c = celerity = \sqrt{gh} .

The integral form of the governing equations is obtained by integrating Eq.1 over a control volume Ω as

$$\frac{\partial}{\partial t} \int_{\Omega} \mathbf{U} dS + \oint_{\partial\Omega} (\mathcal{F} \cdot \mathbf{n}) dL + \int_{\Omega} \mathbf{S} dS = \mathbf{0} \quad (5)$$

where \mathbf{n} = outward-pointing unit vector normal to the cell face $\partial\Omega = (n_x, n_y)$; $\mathcal{F} \cdot \mathbf{n} = \mathbf{E}n_x + \mathbf{F}n_y$ is normal flux vector; dL = length of $\partial\Omega$, dS = area of Ω .

The normal flux vector $\mathcal{F} \cdot \mathbf{n}$ is related to \mathbf{U} through its Jacobian matrix \mathbf{C}_n as

$$\mathbf{C}_n = \frac{\partial (\mathcal{F} \cdot \mathbf{n})}{\partial \mathbf{U}} = \mathbf{A}n_x + \mathbf{B}n_y \quad (6)$$

NUMERICAL MODEL

The first-order accurate FVM model with an unstructured grid (Fig.1) for Eq.5 can be written as

$$\mathbf{U}_i^{t+1} = \mathbf{U}_i^t - \Delta t \left[\frac{1}{V_i} \sum_{k=1}^{N_e} (L_k (\mathcal{F}_k^* \cdot \mathbf{n}_k)) + \mathbf{S}_i \right] \quad (7)$$

where i = index for the cell being computed; t = index for time; k = index for the face of the cell; N_e = total number of faces for a cell; \mathbf{U}_i = average value of \mathbf{U} over the cell i ; \mathbf{S}_i = average value of \mathbf{S} over the cell i ; V_i = area of cell i ; Δt = time increment; L_k = length of the k^{th} face, $\mathcal{F}_k^* \cdot \mathbf{n}_k$ = numerical flux of the k^{th} face.

The numerical flux based on the FDS technique (10) can be written as

$$\mathcal{F}_k^* \cdot \mathbf{n}_k = \frac{1}{2}(\mathcal{F}_R + \mathcal{F}_L) \cdot \mathbf{n}_k - \frac{1}{2}|\widetilde{\mathbf{C}}_{\mathbf{n}_k}|\Delta U \quad (8)$$

where $\mathcal{F}_{R/L} \cdot \mathbf{n}_k$ = normal flux vector on the right/left sides of the k^{th} face; $\widetilde{\mathbf{C}}_{\mathbf{n}_k}$ = approximate Jacobian matrix of the k^{th} face; Δ = operator defined as $\Delta(\bullet) = (\bullet)_R - (\bullet)_L$ where R and L denote the right and left sides of the k^{th} face, respectively.

The approximate Jacobian allows conservative evaluation of the flux vector by $\Delta(\mathcal{F} \cdot \mathbf{n}) = \widetilde{\mathbf{C}}_{\mathbf{n}}\Delta U$. By using concept of approximate Jacobian proposed by Roe (10) for 1D linear systems, the approximate Jacobian may be constructed for 2D cases. This leads to the search of particular averages of velocities and celerity, which are computed as

$$\tilde{u} = \frac{\sqrt{h_L}u_L + \sqrt{h_R}u_R}{\sqrt{h_L} + \sqrt{h_R}}; \quad \tilde{v} = \frac{\sqrt{h_L}v_L + \sqrt{h_R}v_R}{\sqrt{h_L} + \sqrt{h_R}}; \quad \tilde{c} = \sqrt{g \frac{h_L + h_R}{2}} \quad (9)$$

The approximate Jacobian is designed to satisfy the following properties:

$$\Delta U = \sum_{j=1}^3 (\tilde{\alpha}^j \tilde{\mathbf{e}}^j)_k; \quad \Delta(\mathcal{F} \cdot \mathbf{n}) = \widetilde{\mathbf{C}}_{\mathbf{n}_k} \Delta U = \sum_{j=1}^3 (\tilde{\alpha}^j \tilde{\lambda}^j \tilde{\mathbf{e}}^j)_k \quad (10)$$

From Eq.10, the numerical flux can be rewritten as

$$\mathcal{F}_k^* \cdot \mathbf{n}_k = \frac{1}{2}(\mathcal{F}_R + \mathcal{F}_L) \cdot \mathbf{n}_k - \frac{1}{2} \sum_{j=1}^3 (\tilde{\alpha}^j |\tilde{\lambda}^j| \tilde{\mathbf{e}}^j)_k \quad (11)$$

where $\tilde{\lambda}^j$, $\tilde{\mathbf{e}}^j$ = eigenvalues and the right eigenvectors of the approximate Jacobian, respectively; $\tilde{\alpha}^j$ = wave strengths. The eigenvalues can be expressed as

$$\tilde{\lambda}^1 = \tilde{u}n_x + \tilde{v}n_y + \tilde{c}; \quad \tilde{\lambda}^2 = \tilde{u}n_x + \tilde{v}n_y; \quad \tilde{\lambda}^3 = \tilde{u}n_x + \tilde{v}n_y - \tilde{c} \quad (12)$$

The right eigenvectors can be written as

$$\tilde{\mathbf{e}}^1 = \begin{pmatrix} 1 \\ \tilde{u} + \tilde{c}n_x \\ \tilde{v} + \tilde{c}n_y \end{pmatrix}; \quad \tilde{\mathbf{e}}^2 = \begin{pmatrix} 0 \\ -\tilde{c}n_y \\ \tilde{c}n_x \end{pmatrix}; \quad \tilde{\mathbf{e}}^3 = \begin{pmatrix} 1 \\ \tilde{u} - \tilde{c}n_x \\ \tilde{v} - \tilde{c}n_y \end{pmatrix} \quad (13)$$

The wave strengths are given by

$$\begin{pmatrix} \tilde{\alpha}^1 \\ \tilde{\alpha}^2 \\ \tilde{\alpha}^3 \end{pmatrix} = \begin{pmatrix} \frac{\Delta h}{2} + \frac{1}{2\tilde{c}}(\Delta(hu)n_x + \Delta(hv)n_y - \tilde{\mathbf{u}} \cdot \mathbf{n}\Delta h) \\ \frac{1}{\tilde{c}}((\Delta(hv) - \tilde{v}\Delta(h))n_x - (\Delta(hu) - \tilde{u}\Delta(h))n_y) \\ \frac{\Delta h}{2} - \frac{1}{2\tilde{c}}(\Delta(hu)n_x + \Delta(hv)n_y - \tilde{\mathbf{u}} \cdot \mathbf{n}\Delta h) \end{pmatrix} \quad (14)$$

where $\tilde{\mathbf{u}} \cdot \mathbf{n} = \tilde{u}n_x + \tilde{v}n_y$.

The approximate Jacobian defined above does not satisfy the entropy inequality condition. Therefore, Eq.7 might converge to a non-physical solution in case of rarefaction waves. One possible remedy for this problem is to replace the eigenvalue in Eq.11 by a function $\Psi(\tilde{\lambda}^j)$, such as the one proposed by van Leer et al (13). The function $\Psi(\tilde{\lambda}^j)$ is defined as

$$\Psi(\tilde{\lambda}^j) = \begin{cases} |\tilde{\lambda}^j| & \text{if } |\tilde{\lambda}^j| \geq \frac{1}{2}\delta^j \\ \frac{(\tilde{\lambda}^j)^2}{\delta^j} + \frac{1}{4}\delta^j & \text{if } |\tilde{\lambda}^j| < \frac{1}{2}\delta^j \end{cases}; \quad \delta^j = \max(0, 4\Delta\lambda^j) \quad (15)$$

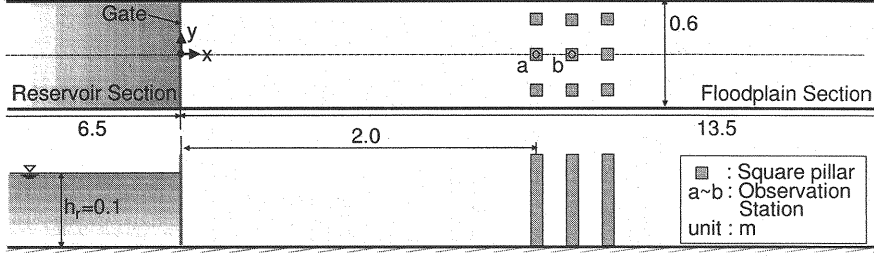


Fig.2 Experimental Set-ups (Flows in a Channel)

The average value of \mathbf{S} is treated in the manner described in (6). \mathbf{S}_i is first split into portions with and without the space derivative terms. Thus,

$$\mathbf{S}_i = \mathbf{S}_{si} + \frac{1}{V_i} \sum_{k=1}^{N_e} \mathbf{S}_k^* \quad (16)$$

where \mathbf{S}_{si} = the vector which contains no derivative term and \mathbf{S}_k^* = upwinded vector which contains a derivative term. \mathbf{S}_{si} and \mathbf{S}_k^* can be written as

$$\mathbf{S}_{si} = \begin{pmatrix} 0 \\ ghS_{fx} \\ ghS_{fy} \end{pmatrix}_i ; \quad \mathbf{S}_k^* = \frac{1}{2} \left(\tilde{\mathbf{S}}_k - \sum_{j=1}^3 \left(\frac{|\tilde{\lambda}^j|}{\tilde{\lambda}^j} \tilde{\beta}^j \tilde{\mathbf{e}}^j \right)_k \right) \quad (17)$$

Finally, $\tilde{\mathbf{S}}_k$ and $\tilde{\beta}^j$ can be expressed as

$$\tilde{\mathbf{S}}_k = \begin{pmatrix} 0 \\ g\tilde{h}(L_k \Delta z_b n_x) \\ g\tilde{h}(L_k \Delta z_b n_y) \end{pmatrix} \quad \text{and} \quad \begin{pmatrix} \tilde{\beta}^1 \\ \tilde{\beta}^2 \\ \tilde{\beta}^3 \end{pmatrix} = \frac{g\tilde{h}(L_k \Delta z_b)}{2\tilde{c}} \begin{pmatrix} 1 \\ 0 \\ -1 \end{pmatrix} \quad (18)$$

BOUNDARY CONDITIONS

Open and Close Boundary

The numerical flux across the cell face lying on the boundary of the computational domain, is calculated by using the following boundary conditions:

The cell face is an open boundary when there is flow across the cell face. This boundary condition is determined according to the type of local flow regime, which is either sub- or super-critical. For sub-critical flow, the flow depth or unit-width discharge normal to the cell face is given. When the flow depth h_R is given, velocity normal to the cell face $\mathbf{u} \cdot \mathbf{n}_R$ is obtained from Eq.19. On the other hand, when the unit-width discharge q_n is given, h_R can be solved from the Eq.20.

$$(\mathbf{u} \cdot \mathbf{n})_R = (\mathbf{u} \cdot \mathbf{n})_L + 2(c_L - c_R) \quad (19)$$

$$2c_R^3 - ((\mathbf{u} \cdot \mathbf{n})_L + 2c_L)c_R^2 + gq_n = 0 \quad (20)$$

For super-critical flow, at the inflow boundary, both flow depth and velocity normal to the face are specified. At the outflow boundary, no external condition is necessary.

At the closed boundary, the flow across the cell face is set to zero. Therefore,

$$(\mathbf{u} \cdot \mathbf{n})_R = -(\mathbf{u} \cdot \mathbf{n})_L ; h_R = h_L \quad (21)$$

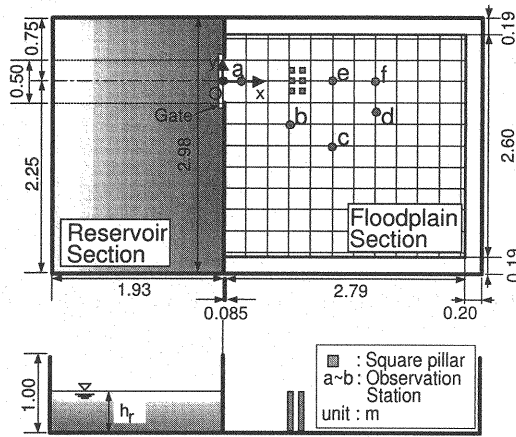


Fig.3 Experimental Set-ups (Flows in a Floodplain)

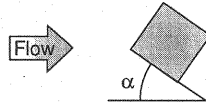


Fig.4 Definition of Angle of Attack α

Treatment of Dry-Bed

A very small flow depth h_v is assumed in dry cells while velocities u and v are set to zero. In order to prevent an unrealistically high friction slope at very small flow depths, a tolerance depth h_c is specified and friction slopes S_{fx} and S_{fy} are set to zero as long as the flow depth in a cell remains less than h_c . Based on numerical experiments, the values of h_v and h_c are set to 0.00001m and 0.001m, respectively.

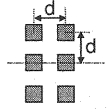
EXPERIMENTS

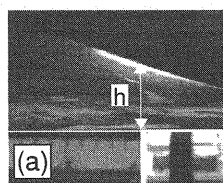
Two different experimental set-ups were used: a straight channel (Fig.2) and a floodplain (Fig.3). The experimental set-ups in both cases consist of a reservoir section and a floodplain section separated by a gate-fitted wall. The bed in both cases was horizontal and their Manning's roughness coefficient was 0.01. The floodplain in both cases was initially dry. The presence of structures, such as buildings, was modeled by placing the square pillars (0.06m wide, 0.2m tall) in the floodplain. The angle of attack of a square pillar was defined as shown in Fig.4. Experimental conditions are shown in Table 1.

For experiments in the channel, the length and width of the reservoir section are 6.5m and 0.6m, respectively. The length and width of the floodplain sections are 13.5m and 0.6m, respectively. The width of the gate was the same as that of the channel. The number of rows of the square pillars used varied from 1 to 3, and the angle of attack of the pillars was changed to 0° , 15° , 30° and 45° . The initial depth in reservoir section was 0.1m. Furthermore, the flow depths were observed at each observation stations.

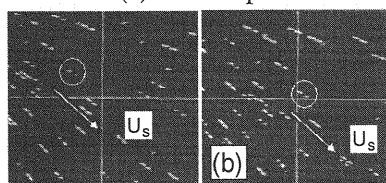
For experiments in a floodplain, the length and width of the reservoir section was 2.0m and 3.0m, respectively. The length and width of floodplain section was 3.0m and 3.0m, respectively. The gate was 0.5m wide and was located at 0.75m from the left-side end of the wall separating the

Table1 Experimental Conditions

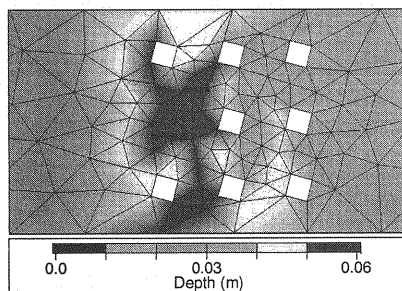
	Channel					Floodplain																														
Arrangement of Square Pillars	CASE 1	CASE 2	CASE 3	CASE 4	CASE 5																															
Square Pillars Spacing d (m)	0.18					0.12																														
Angle of Attack α (deg)	0, 15, 30, 45					0																														
Initial Depth in Reservoir Sections h_r (m)	0.1					0.2																														
Observed Data	Flow Depth					Flow Depth Surface Velocities																														
Locations of Observation Stations	<table border="1"><thead><tr><th></th><th>x (m)</th><th>y (m)</th></tr></thead><tbody><tr><td>a</td><td>2.03</td><td>0.00</td></tr><tr><td>b</td><td>2.21</td><td>0.00</td></tr></tbody></table>						x (m)	y (m)	a	2.03	0.00	b	2.21	0.00	<table border="1"><thead><tr><th></th><th>x (m)</th><th>y (m)</th></tr></thead><tbody><tr><td>a</td><td>0.29</td><td>0.00</td></tr><tr><td>b</td><td>0.84</td><td>-0.50</td></tr><tr><td>c</td><td>1.34</td><td>-0.75</td></tr><tr><td>d</td><td>1.84</td><td>-0.35</td></tr><tr><td>e</td><td>1.35</td><td>0.00</td></tr><tr><td>f</td><td>1.84</td><td>0.00</td></tr></tbody></table>		x (m)	y (m)	a	0.29	0.00	b	0.84	-0.50	c	1.34	-0.75	d	1.84	-0.35	e	1.35	0.00	f	1.84	0.00
							x (m)	y (m)																												
						a	2.03	0.00																												
						b	2.21	0.00																												
							x (m)	y (m)																												
						a	0.29	0.00																												
b	0.84	-0.50																																		
c	1.34	-0.75																																		
d	1.84	-0.35																																		
e	1.35	0.00																																		
f	1.84	0.00																																		



(a) Flow Depth



(b) Surface Velocities

Fig.5 Measuring Method for Flow Depth and Surface Velocities**Fig.6** Examples of Grid Arrangement and Computation Results of the Flow Depth (Flows in a Channel, CASE1, $\alpha=15^\circ$, $t=3.5$ seconds)

reservoir section from the floodplain section (Fig.3). The number of rows of square pillars and the angle of attack of the pillars were not changed. The initial depth in reservoir section was 0.2m. The flow depths and surface velocities were observed at each observation station.

A dam-break flood flow was produced by opening the gate instantaneously. A water surface profile visualized by a laser light sheet and was recorded by means of a digital VTR. Flow depths were obtained by analyzing the recorded images with a computer as shown in Fig.5(a). Surface velocities were obtained by analyzing the motions of foam polystyrenes floating on water surface with PTV(Particle Tracking Velocimetry) as shown in Fig.5(b). From these measurements, the depth-averaged velocities were calculated from $U_a = 0.92U_s$, which is a relationship between the depth-average velocity vector U_a and the surface velocity vector U_s , obtained from an experiment results of 1D dam-break flows (1). Each experiment was repeated at least 4 times under the same conditions in order to obtain reliable data.

MODEL VERIFICATION

Flows in a Channel

Examples of grid arrangement and computational results of the flow depth around the pillars for CASE 3 with $\alpha = 15^\circ$ at 3.5 seconds after opening the gate are shown in Fig.6. The figure shows that the rise of the flow depth around 1st- and 2nd-rows of pillars propagates upstream.

Fig.7 compares the computed depths with observed data of CASE 1 ~ CASE 3 at each angle of attack. It shows that the computed depths coincide satisfactorily with the observed data in all cases. The computed results reproduce the following observed phenomena: (1) there is a rise of flow depth from the arrival time of the wave front up to 5.0 seconds and after that the flow depth remains largely unchanged. (2) Depending on the angle of attack α , the part of channel width blocked by the pillars is changed. Accordingly, the rise of flow depth in front of the pillars also changed. (3) The difference in flow depth between CASE 1 and CASE 2 is wider than the difference between CASE 2 and CASE 3. It should be noted that at the observation stations for CASE 1, the discrepancy between the computed and the observed depths is wider than the other stations. This may be due to the effects of a complicated streamline curvature in the vertical, which is stronger for CASE 1.

A trend similar to CASE 1 can also be revealed in CASE 4, and for the first 5.0 seconds in CASE 5(Fig.8). At 5.0 seconds after opening the gate in CASE 5, the computed depths coincide with the observed depths. The discrepancies in the flow depth between CASE 4 and CASE 5 are significant up to 3.0 or 4.0 seconds after opening the gate. This provides evidence that the effects of the last row of pillars in CASE 5 become significant after 3.0 or 4.0 seconds from the opening of the gate.

Flows in a Floodplain

Examples of grid arrangement and computation results of the flow depth around the pillars at 2.0 seconds from opening the gate are shown in Fig.9. This figure shows that the flood flows obstructed by the pillars are deflected, and consequently the flow depth in front of the pillars rises.

Fig.10 compares the computed depths with observed data at each observation station. At the stations *a*, *e* and *f* on the gate center axis, it is observed that the flow depth rises suddenly in the beginning and then drops sharply. Thereafter the flow depth continues to decrease. At the station *a* near the gate, the computed depths coincide closely with the observed data except for the initial 3.0 seconds after opening the gate. At this time, the computed depths are lower than the observed data. At the stations *e* and *f*, the computed depths mostly match with the observed data except for the initial 2.0 seconds after opening the gate. In this period, the computed depths are slightly lower than the observed data. The discrepancy between the computed and the observed values at the station *a* is wider than the values at stations *e* and *f*. This provides evidence of the effects of streamline curvature in the vertical, which is stronger near the breach sections. The reason for the discrepancy between the computed and observed values is that the governing equations are not

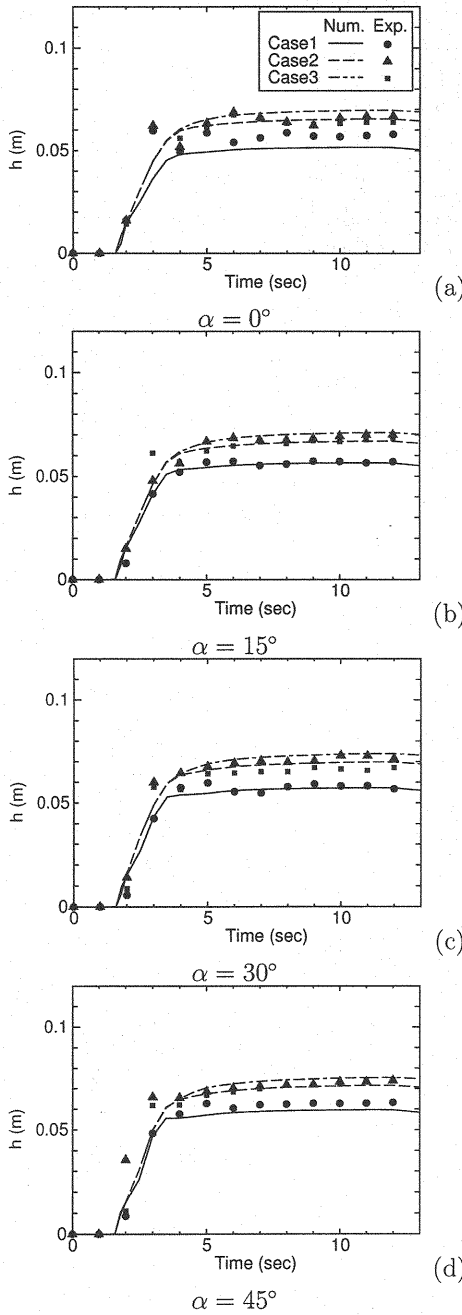


Fig.7 Comparison of Computed and Observed Depth at the Station a (CASE1~CASE3)

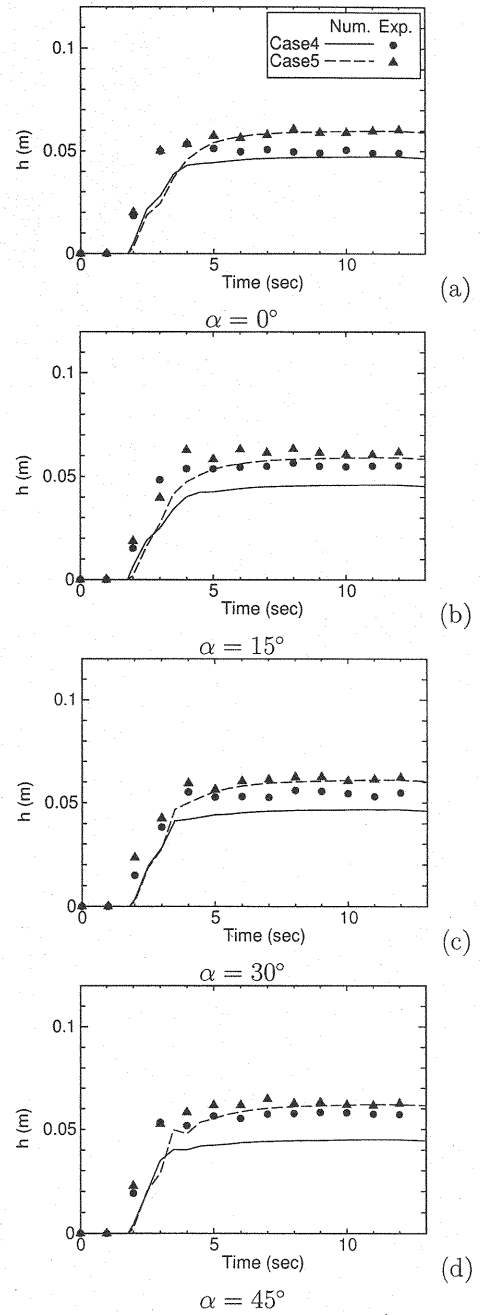


Fig.8 Comparison of Computed And Observed Depth at the Station b (CASE4, CASE5)

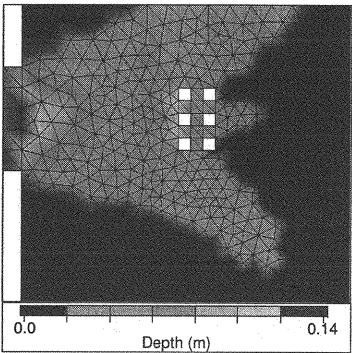


Fig.9 Examples of Grid Arrangement and Computation Results of the Flow Depth (Flows in a Floodplain, $t=2.0$ seconds)

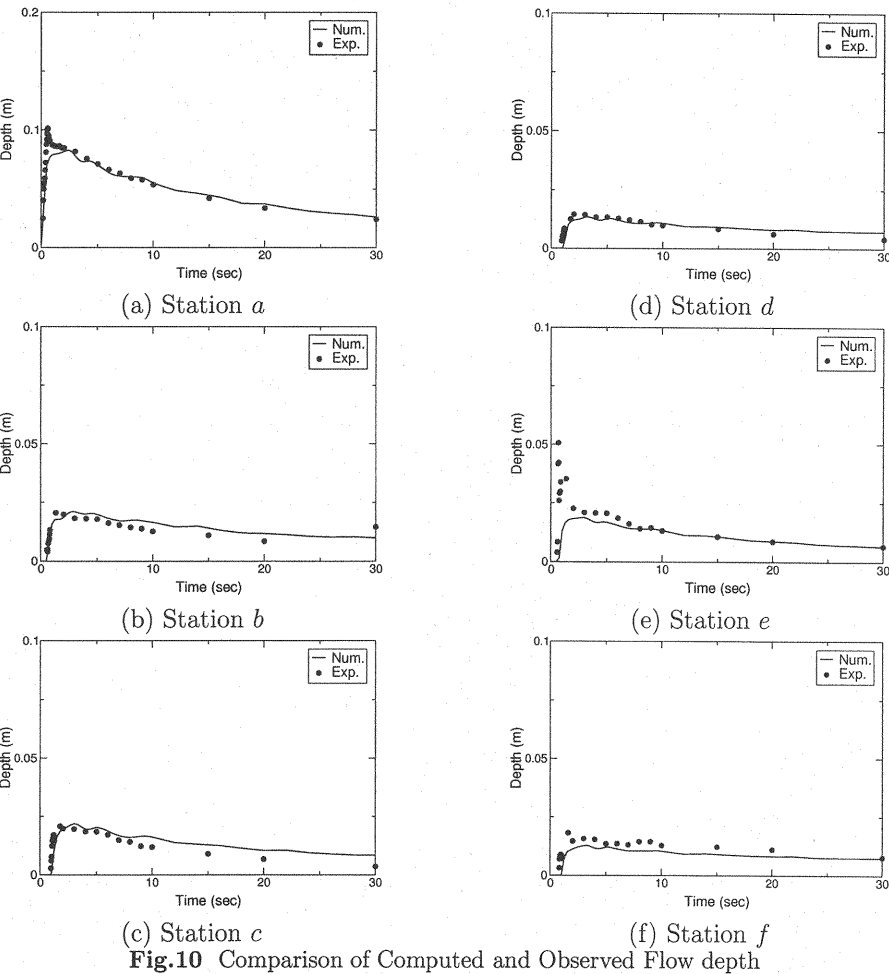


Fig.10 Comparison of Computed and Observed Flow depth

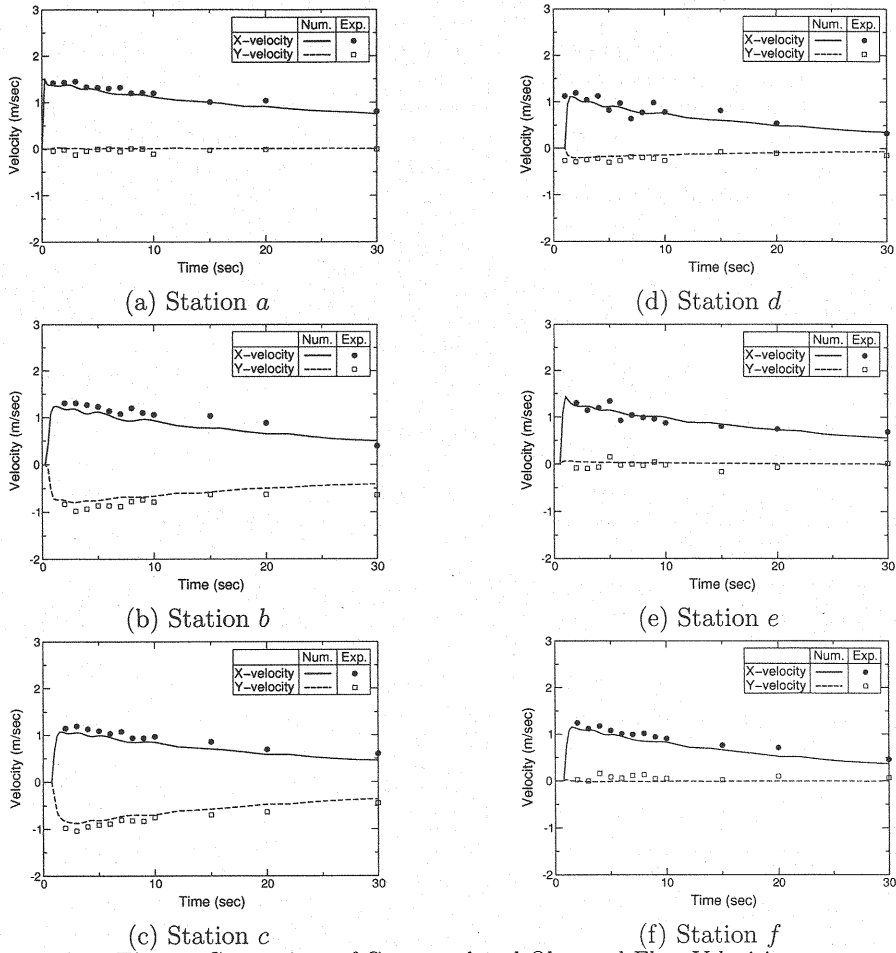


Fig.11 Comparison of Computed and Observed Flow Velocities

capable of handling these effects. At the stations *b*, *c* and *d*, which are away from the gate center axis, the flow depth rises suddenly in the beginning and continues to decrease thereafter. The computed depths mostly coincide with the observed data.

Fig.11 compares the computed depth-averaged velocities with observed data at each observation station. The observed velocities at all stations rise to their maximum in the beginning and continue to decrease at a later period. At the stations *a*, *e* and *f*, the observed *y*-velocity is nearly equal to 0. The computed results mostly reproduce the observed data. At the stations *a*, *e* and *f*, the discrepancy between the computed results and observed ones is due to the same reason as that of flow depths. At other stations, a slight discrepancy between computed and observed values may be identified. This is mainly due to the fact that approximation of the dry-bed was made in very shallow water.

The above findings demonstrate the proposed model reproduces the observed depth as well as velocities of 2D dam-break flood waves propagating on a horizontal dry-bed with the square pillars with reasonable accuracy.

CONCLUSION

An accurate FVM numerical model for 2D flood flows which can handle a complicated floodplain geometry is presented in this work. The model is based on the FDS technique which satisfies

conservative property and incorporates signal propagation. An unstructured triangular grid system is employed for efficient handling of complicated floodplain geometriy. For a completely accurate verification of the model, experiments of dam-break flood waves propagating in a channel as well as a floodplain with square pillars, which model structures, were conducted. The experimental data on the flow depth and surface velocities were obtained by using an image analysis and PTV, respectively. The model was verified against the experimental data and was found to reproduce the observed depth and velocities with reasonable accuracy.

ACKNOWLEDGMENT

This study was supported by the Grant in Aid for Scientific Research of the Ministry of Education and Culture, Japan, under Grant Number(B)11450190. The authors wish to thank the contribution made by Mr. Toshihiko KOBAYASHI and Mr. Kazumasa OTA to our work.

REFERENCES

1. Akiyama, J., Shige-da, M., Kobayashi, T. and Oota, K.: Hydrodynamic force exerting on a square pillar in unsteady free surface flows, *Annual Journal of Hydraulic Engineering*, Vol. 46, pp. 1205–1210, 2002.
2. Alcrudo, F. and Garcia-Navarro, P.: A High-resolution Godunov-type scheme in finite volumes for the 2D shallow-water equations, *International Journal for Numerical Methods in Fluids*, Vol. 16, pp. 489–505, 1993.
3. Ariga, T.: An experimental study on presumption of inundation area caused by riverdyke breaking (I) (A proposal of an inundation-model), *Proceedings of the school of Engineering Tokai University*, No. 8, pp. 133–178, 1977 (in Japanese).
4. Bellos, C. V., Soulis, J. V. and Sakkas, J. G.: Computation of 2-dimensional dam-break induced flows, *Advances in Water Resources*, Vol. 14, No. 1, pp. 31–41, 1991.
5. Fraccarollo, L. and Toro, E. F.: Experimental and numerical assessment of the shallow water model for two-dimensional dam-break type problems, *Journal of Hydraulic Research*, Vol. 33, No. 6, pp. 843–864, 1995.
6. Jha, A. K., Akiyama, J. and Ura, M.: Flux-difference splitting schemes for 2D flood flows, *Journal of hydraulic Engineering*, ASCE, Vol. 126, No. 1, pp. 33–42, 2000.
7. Kawaike, K., Inoue, K. and Toda, K.: Application of unstructured meshes to inundation flow analysis in urban area, *Annual Journal of Hydraulic Engineering*, JSCE, Vol. 44, pp. 461–466, 2000.
8. Kawaike, K., Inoue, K., Toda, K. and Nakai, T.: Effect of sediments yield on inundation flow analysis in hillside cities, *Annual Journal of Hydraulic Engineering*, JSCE, Vol. 45, pp. 883–888, 2001.
9. Mingham, C. G. and Causon, D. M.: High-resolution finite-volume method for shallow water flows, *Journal of Hydraulic Engineering*, ASCE, Vol. 124, No. 6, pp. 605–614, 1998.
10. Roe, P. L.: Approximate Riemann solvers, parameter vectors and difference schemes, *Journal of Computational Physics*, Vol. 43, pp. 357–372, 1981.
11. Sleigh, P. A., Gaskell, P. H., Berzins, M. and Wright, N. G.: An unstructured finite-volume algorithm for predicting flow in rivers and estuaries, *Computers & Fluids*, Vol. 27, No. 4, pp. 479–508, 1998.
12. Takahashi, T. and Nakagawa, H.: Behavior of the over land flood flows in the modeled urban area, *Annals of the Disaster Prevention Research Institute, Kyoto University*, Vol. 26B-2, pp. 245–259, 1983 (in Japanese).
13. van Leer, B., Lee, W. T. and Powell, K. G.: Sonic-point capturing, *AIAA 9th Computational Fluid Dynamics Conference*, 1989.

APPENDIX-NOTATION

The following symbols are used in this paper:

\mathbf{U}	=	flow vector;
\mathbf{E}, \mathbf{F}	=	flux vectors;
\mathbf{S}	=	vector containing source and sink terms;
h	=	flow depth;
u, v	=	velocities along x- and y-direction, respectively;
g	=	acceleration due to gravity;
S_{ox}, S_{oy}	=	bed slopes along x- and y-direction, respectively;
S_{fx}, S_{fy}	=	friction slopes along x- and y-direction, respectively;
n	=	Manning's roughness coefficient;
c	=	celerity($=\sqrt{gh}$);
\mathbf{n}	=	outward-pointing unit vector normal to cell face = $((n_x, n_y))$;
$\mathcal{F} \cdot \mathbf{n}$	=	normal flux vector;
i	=	index for a cell;
t	=	index for time;
k	=	index for a cell face;
N_e	=	total number of cell face;
U_i	=	average value of \mathbf{U} over the cell i ;
S_i	=	average value of \mathbf{S} over the cell i ;
V_i	=	area of cell i ;
Δt	=	time increment;
L_k	=	length of the k^{th} face;
$\mathcal{F}_k^* \cdot \mathbf{n}_k$	=	numerical flux of the k^{th} face;
Δ	=	operator defined as $\Delta(\bullet) = (\bullet)_R - (\bullet)_L$;
C_{nk}	=	approximate Jacobian matrix of the k^{th} face;
$\tilde{\lambda}^j, \tilde{\mathbf{e}}^j$	=	eigenvalues and right eigenvectors, respectively; and
$\tilde{\alpha}^j$	=	wave strengths.

(Received August 23, 2001 ; revised February 22, 2002)